Astron. Astrophys. 361, 1058–1072 (2000)

ASTRONOMY AND ASTROPHYSICS

A ridge of recent massive star formation between Sgr B2M and Sgr B2N

P. de Vicente[1], **J. Martín-Pintado**[1], **R. Neri**[2], **and P. Colom**[3]

[1] Observatorio Astronómico Nacional, Apartado 1143, 28080 Alcalá de Henares, Spain
[2] Institut de Radioastronomie Millimetrique, Rue de la Piscine, St. Martin de Heres, France
[3] Observatoire de Meudon, Meudon, Paris, France

Received 27 March 2000 / Accepted 11 August 2000

Abstract. We present single dish and interferometric maps of several rotational transitions of HC_3N vibrationally excited levels towards Sgr B2. HC_3N is a very suitable molecule to probe hot and dense regions (hot cores) affected by high extinction since its vibrational levels are mainly excited by mid-IR radiation. The single dish maps show, for the first time, that the HC_3N vibrationally excited emission (HC_3N*) is not restricted to Sgr B2M and N but extended over an area $40'' \times 20''$ in extent. We distinguish four bright clumps (Sgr B2R1 to B2R4) in the ridge connecting the main cores Sgr B2M and Sgr B2N, and a low brightness extended region to the west of the ridge (Sgr B2W). The physical properties and the kinematics of all hot cores have been derived from the HC_3N* lines. Our high angular resolution images show that the Sgr B2N hot core breaks in two different hot cores, Sgr B2N1 and N2, with different radial velocities and separated by $\sim 2''$ in declination. We find that the excitation of the HC_3N* emission in all hot cores can be represented by a single temperature and that the linewidth of the HC_3N* rotational lines arising from different vibrational levels systematically decreases as the energy of the vibrational level increases. The systematic trend in the linewidth is likely related to the increase of the velocity as the distance to the exciting source increases. We have developed a simple model to study the excitation of the HC_3N vibrational levels by IR radiation. We find that the single excitation temperature can be explained by high luminosities of embedded stars ($\sim 10^7$ $L_\odot$) and small source sizes ($\sim 2-3''$). The estimated clump masses are 500 $M_\odot$ for Sgr B2M, 800 $M_\odot$ for Sgr B2N and 10-30 $M_\odot$ for Sgr B2R1 to B2R4. Luminosities are $1-2\,10^6$ $L_\odot$ for Sgr B2R1-B2R4 and Sgr B2M and 10^7 $L_\odot$ for Sgr B2N. We estimate HC_3N abundances of $5\,10^{-9}$ for Sgr B2M and Sgr B2N2 and 10^{-7} for the rest of the hot cores. The different HC_3N abundances in the hot cores reflect different stages of evolution due to time dependent chemistry and/or photo-dissociation by UV radiation from nearby HII regions. According to the mass and the luminosity of the different hot cores, we propose that Sgr B2M and B2N contain a cluster of 20–30 hot cores, each like that in Orion A, a number similar to the UC HII regions already detected in the region. The Sgr B2R1-B2R4 hot cores represent isolated formation of massive stars.

Send offprint requests to: P. de Vicente (vicente@oan.es)

Key words: ISM: clouds – ISM: H II regions – ISM: kinematics and dynamics – ISM: molecules

1. Introduction

Recent massive star formation in the Galaxy is commonly recognized by signposts, like UC HII regions, H_2O masers, near and mid infrared emission and hot and dense condensations containing molecules and dust. These condensations are known as hot cores and represent a relatively early phase of massive star formation.

The Sagittarius B2 molecular cloud, located near the Galactic center, at a distance of 7.1 kpc (Reid et al., 1988) is one of the most active regions of massive star formation in the Galaxy. It contains two cores, Sgr B2M and Sgr B2N, which show all the typical signposts of very luminous embedded young stellar objects. Sgr B2M and Sgr B2N, are very strong IR emitters (Thronson & Harper, 1986; Goldsmith et al., 1987; Goldsmith et al., 1990), they contain several compact and ultra compact HII regions (Gaume & Claussen, 1990; Gaume et al., 1995; de Pree et al., 1998), hot cores (Vogel et al., 1987; Mehringer & Menten, 1997; Martín-Pintado et al., 1990; de Vicente et al., 1997) and H_2O masers (Reid et al., 1988; Kobayashi et al., 1989).

The Sgr B2N and Sgr B2M hot cores have already been studied for example, in NH_3 (Vogel et al., 1987), H_2CO (Martín-Pintado et al., 1990), CH_3CN (de Vicente et al., 1997) and C_2H_3CN (Liu & Snyder, 1999). Different molecules seem to give different physical properties and kinematics for the hot cores. This is because different tracers require different excitation conditions and because of the complexity of the region. Cyanoacetylene (HC_3N) is a very suitable molecule to probe the physical properties and kinematics in the hot cores since it has several vibrational states which lie in the range between 300 and 1000 K, which are only excited by IR radiation in the hot cores. Thus the vibrationally excited lines of HC_3N probe regions with strong emission in the mid-IR.

Since the detection of the rotational line from the vibrational v7=1 state by Goldsmith et al. (1982) in Orion, rotational lines from vibrational states arising from other sources and from

other vibrational states have been discovered. Most of the studies of vibrationally excited HC_3N (hereafter HC_3N*) emission towards Sgr B2 have been made with low angular resolution (Goldsmith et al., 1985b; Martín-Pintado et al., 1986) and only towards Sgr B2M and Sgr B2N.

Recently Martín-Pintado et al. (1999) have found that recent massive star formation in the stage of hot cores is not only restricted to Sgr B2M, Sgr B2N, and Sgr B2S but is also present in the envelope of Sgr B2. These new hot cores are less massive than those in Sgr B2M and Sgr B2N. This suggests that recent massive star formation similar to that in Orion A might occur over more extended regions than the main cores Sgr B2M, B2N and B2S. The aim of this paper is twofold: to obtain a global picture of massive star formation between the main cores Sgr B2M and B2N and to study in detail the hot cores Sgr B2M and Sgr B2N. To study in detail the physical properties and the kinematics of the hot cores in Sgr B2M and Sgr B2N, we present interferometric observations of several HC_3N* lines. The global picture of star formation has been obtained from mapping several HC_3N* lines obtained with the IRAM 30m dish. This map has revealed for the first time the presence of a ridge of hot cores similar to that in Orion A.

2. Observations

2.1. Single dish observations

We have carried out single dish observations of different rotational lines of HC_3N and its isotopic species $HC^{13}CCN$ and $HCC^{13}CN$ from the ground and vibrational states with the IRAM 30m telescope at Pico de Veleta (Spain) towards the regions containing the hot cores Sgr B2M and Sgr B2N. We observed the J=10–9 (3.3 mm), J=12–11 (2.9 mm), J=15–14 (2.2 mm), J=16–15 (2 mm), J=17–16 (1.9 mm) and J=24–23 (1.3 mm). The Half Power Beam Width (HPBW) of the telescope at 3, 2 and 1.3 mm was $26''$, $17''$ and $12''$. We used three SIS receivers to observe simultaneously the 3, 2 and 1.3 mm lines. Most of the observations were made with the receivers tuned to SSB mode with an image rejection of 7 to 9 dB. The observations were performed in a position switching mode, taking the reference position $10'$ off the on-sources in right ascension. The line intensity calibration was established measuring a cold and ambient temperature load of known temperatures. The line intensities have been converted to main beam temperatures by using beam efficiencies of 0.6 for 3 and 2mm and 0.45 for 1.3 mm and a forward eficciency of 0.9 for all wavelengths. As spectrometers we used two 512 MHz filter banks and one 1024 channel autocorrelator. The velocity resolution provided by the spectrometers were 3.3, 2.7, 1.9 and 0.4 kms^{-1} for the 3.3, 2.9, 2 and 1.3 mm lines respectively.

In order to determine the spatial extension of the HC_3N* emission, we mapped a region of $50''\times 50''$ around Sgr B2M and Sgr B2N in the J=16–15,3v7,1e and the J=24–23,3v7,1e HC_3N lines with a $5''$ spacing. Simultaneous with the J=16,1e-15,3v7,1e line we observed the $H_2^{13}CO$ 2(1,1)–2(1,0) transition which is seen in absorption towards both continuum sources and allowed to check the pointing relative to the continuum sources in our map. Observations towards the most intense condensations in the previous map were also made in the J=10-9,1v7,1f 1v6,1e and 1v5,1f transitions and in the J=24-23,1v7,1f transition.

Table 1. Instrumental parameters for the PdBI observations

Parameter	Value
Sources observed	2
Total time on sources	1.6 hours
Central sky frequency	91.155 GHz
Primary beam (HPBW)	$56''$
Synthesized beam (HPBW) (B2M)	$10.5'' \times 4.9''$ PA: 0^o
Synthesized beam (HPBW) (B2N)	$12.2'' \times 4.4''$ PA: -14^o
Interferometer configuration	Dc (W05,E03,N05)
Flux density calibrator	1730-130 (14 Jy)
Phase and Band Pass calibrators	1730-130 (14 Jy)
	1830-21 (3.2 Jy)
Phase center position J2000 (B2M)	17:47:20.3 -28:23:07
Phase center position J2000 (B2N)	17:47:20.3 -28:22:19
Absolute position error	$\pm\ 0.4''$

2.2. Interferometric observations

Since the single dish HC_3N* maps showed this emission to be unresolved towards the Sgr B2M and Sgr B2N cores we used the IRAM interferometer at Plateau de Bure, France, to map the emission with higher angular resolution. We performed two snapshots of Sgr B2M and Sgr B2N in July 1995 with three antennas. The instrumental parameters for the Plateau de Bure interferometer observations are summarized in Table 1. Observations were made at 91.2 GHz in order to measure simultaneously the J=10–9,1v5,1f, J=10–9,1v6,1e, J=10–9,1v7,1e and J=10–9,1v7,1f transitions. We used the source 1730-13 (14 Jy) as the flux density and bandpass calibrator and 1830-21 (3.2 Jy) as the phase calibrator.

3. Results

3.1. Single dish

Fig. 1 shows a map of the integrated intensity of the J=24–23,3v7,1e HC_3N line. This line was observed with the receiver tuned in nearly double side band, the relative gain for the image band was only 0.2. The integrated emission also contains the J=25–24,1v7,1e and 1v6,1e lines which were observed in the image band. The map shows the morphology of the HC_3N^* in the region. The HC3N* emission is dominated by the already known massive hot cores associated with Sgr B2M and Sgr B2N (Goldsmith et al., 1987; Vogel et al., 1987; Lis & Goldsmith, 1991; Martín-Pintado et al., 1990). The map also shows for the first time the presence of a ridge of HC_3N* emission connecting the Sgr B2M and B2N hot cores, and an extended low brightness emission to the west of the ridge. The HC_3N* ridge is unresolved in the east-west direction. For further study we have considered four sources labelled as B2R1, B2R2, B2R3 and B2R4 (see Fig. 1). The extended component

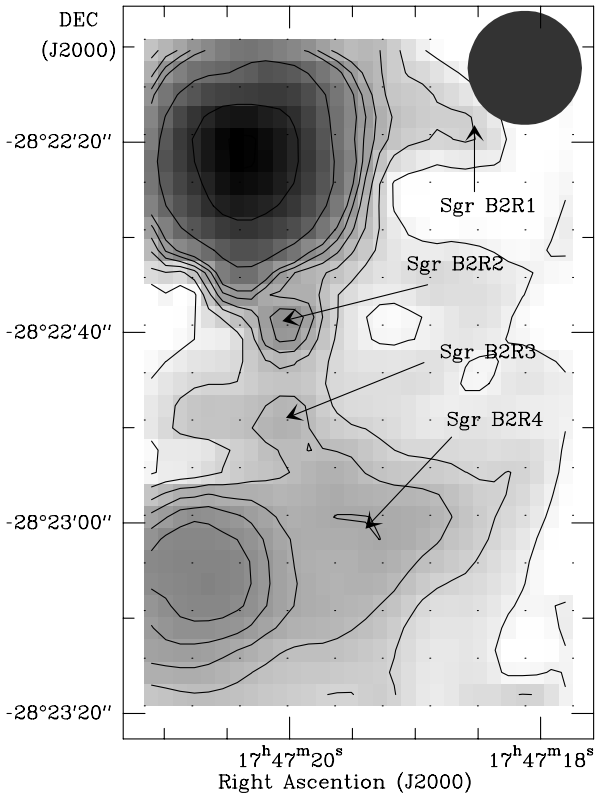

Fig. 1. Map obtained at the 30m radio telescope for the integrated intensity of HC_3N J=24-23,3v7,1e transition (see Sect. 3.1 for an additional explanation). Levels are 5, 10 15, 20, 25, 30, 50, 100, and 150 K kms^{-1} using antenna temperature scale. We have labeled the new hot cores along the ridge as Sgr B2R1, B2R2, B2R3 and B2R4. The filled circle in the upper right corner shows the beam size.

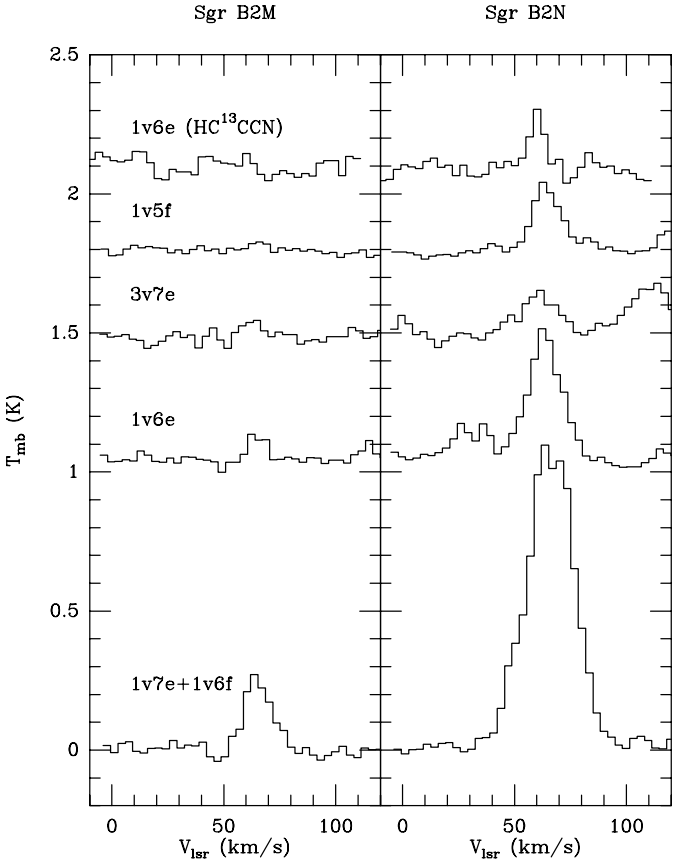

Fig. 2. Spectra taken at the 30m radio telescope for the HC_3N J=10-9 transition in different vibrational excited levels, towards Sgr B2M and Sgr B2N. The upper panel shows the spectra of the J=10-9 line of $HC^{13}CCN$ in the 1v6,1e vibrational level.

has a size of $\sim 30''$, and hereafter will be referred to as Sgr B2W.

Fig. 2 shows typical profiles of the J=10–9 line of HC_3N* and $HC^{13}CCN$ for several vibrational states towards Sgr B2M (left panel) and Sgr B2N (right panel) taken at the 30m radio telescope. This figure clearly shows the difference in the excitation of the material in the Sgr B2M and Sgr B2N hot cores. Table 2 summarizes the single dish results. The line parameters in this table have been derived by fitting a Gaussian profile to the lines. As intensity scale we have used the main beam temperature because the emission region is in all cases smaller than the telescope beam.

The rotational transitions of the vibrational states appear in pairs, due to the level degeneracy, separated in frequency by tenths of MHz. This feature has been used to aid in the determination of the parameters of the Gaussian fits when one of the transition pairs appears contaminated by more intense lines. In those cases in which we have used the width of the pair transition, the error associated with the fitted parameter of the contaminated line is indicated in Table 2 as 0. The line widths towards Sgr B2N and Sgr B2M depend on the energy of levels involved in the transition. The line width increases as the energy of the levels involved increases.

Table 3 summarizes the Gaussian fits to the $HC^{13}CCN$ and $HCC^{13}CN$ single dish profiles at the ground and vibrational excited levels. The frequencies of the $HC^{13}CCN$ and $HCC^{13}CN$ lines have been calculated using the expressions given by Wyrowski et al. (1999). Due to line confusion we have only used those transitions which were not blended with other lines. The rotational transitions for the vibrational ground state of $HC^{13}CCN$ and $HCC^{13}CN$ are separated a few MHz and can be observed simultaneously. Both lines have similar intensities and widths indicating that both isotopic substitutions have the same abundance, within the calibration errors.

From the intensities of the main isotope and from those of the ^{13}C isotope, and assuming an isotopic ratio $^{12}C/^{13}C$ of 20 for the Galactic center (Wilson & Rood, 1994), we estimate the opacity depth of the main isotope HC_3N lines. Towards Sgr B2M the opacities of the main isotope rotational transitions in the ground vibrational state are between 0.4 and 0.6, while for the vibrational levels we obtain an upper limit of 0.1. Therefore all HC_3N^* lines in the Sgr B2M hot core are optically thin. On the other hand the opacity of the HC_3N* lines towards Sgr B2N is ~ 4.5. This means that $HC^{13}CCN$ and $HCC^{13}CN$ lines in the ground states are also probably optically thick and cannot be used to determine the opacity of the main isotope transitions.

Table 2. Fits for different HC_3N transitions towards Sgr B2M and Sgr B2N. Single dish observations

	Sgr B2M					Sgr B2N			
Transition	E_{upp} (K)	T_{mb} (K)	v ($km\,s^{-1}$)	Δv ($km\,s^{-1}$)	Area ($K\,km\,s^{-1}$)	T_{mb} (K)	v ($km\,s^{-1}$)	Δv ($km\,s^{-1}$)	Area ($K\,km\,s^{-1}$)
10–9	24.1	7.45	59.2(0.1)	19.3(0.3)	153.0(1.9)	7.24	66.5(0.1)	23.6(0.1)	182.0(0.7)
10,1e–9,1e 1v5	978.3					0.43	62.3(0.6)	13.9(1.0)	6.4(0.5)
10,1f–9,1f 1v5	978.3	0.04	65.5(1.3)	7.3(2.5)	0.3(0.1)	0.32	63.9(0.8)	15.3(1.9)	5.2(0.6)
10,1e–9,1e 1v6	741.3	0.09	64.8(0.6)	11.3(1.4)	1.0(0.1)	0.54	63.6(0.7)	17.6(1.7)	10.1(0.8)
10,1f–9,1f 1v6	741.3	0.07	62.8(0.0)	8.4(0.0)	0.7(0.0)	0.49	63.6(0.1)	16.1(1.1)	8.3(0.5)
10,1e–9,1e 1v7	344.1	0.36	64.1(0.3)	11.7(0.8)	4.4(0.3)	1.13	63.0(0.1)	23.0(0.6)	27.5(0.7)
10,0–9,0 2v7	662.1					0.22	64.0(1.0)	24.2(1.3)	5.6(0.4)
10,2e–9,2e 2v7	664.7					0.22	63.9(0.0)	24.2(0.0)	5.6(0.0)
10,2f–9,2f 2v7	664.7					0.22	64.0(0.0)	24.2(0.0)	5.6(0.0)
10,1e–9,1e 3v7	980.6	0.08	62.6(1.2)	8.9(2.2)	0.7(0.2)	0.23	61.1(1.4)	14.0(0.0)	3.5(0.4)
12–11	34.1	9.19	59.4(0.1)	18.1(0.3)	177.1(2.3)	8.33	66.0(0.1)	22.1(0.2)	196.3(1.3)
12,1e–11,1e 1v5	988.3					0.78	63.4(0.7)	15.8(1.4)	13.1(1.1)
12,1f–11,1f 1v5	988.3					0.75	63.0(0.0)	12.0(0.0)	9.6(0.0)
12,1e–11,1e 1v6	751.3	0.16	62.9(1.0)	11.6(2.5)	2.0(0.3)	0.60	62.4(0.5)	19.2(1.2)	12.1(0.6)
12,1f–11,1f 1v6	751.4	0.15	63.0(0.0)	11.6(0.0)	1.9(0.0)	0.90	64.0(0.0)	15.8(0.0)	15.1(1.6)
12,1e–11,1e 1v7	354.1	0.68	62.7(0.0)	17.0(0.0)	12.3(1.1)	2.11	62.2(0.0)	26.0(0.0)	58.5(0.0)
12,1f–11,1f 1v7	354.1	0.87	61.1(2.0)	17.0(0.0)	15.7(2.1)	1.75	62.2(1.4)	28.2(3.4)	60.8(4.5)
12,0–11,0 2v7	672.2					0.80	62.9(2.7)	17.2(2.7)	13.8(2.1)
12,1e–11,1e 2v7	672.2					0.80	62.9(0.0)	13.8(0.0)	17.2(0.0)
12,1f–11,1f 2v7	672.2					0.80	62.9(0.0)	13.8(0.0)	17.2(0.0)
15–14	52.4	7.31	61.4(0.1)	17.0(0.3)	131.9(2.3)	7.62	64.5(0.3)	20.4(0.9)	165.4(5.5)
15,1e–14,1e 1v5	1006.7					0.88	63.0(0.0)	14.1(0.0)	15.0(0.0)
15,1f–14,1f 1v5	1006.7	0.14	63.0(0.0)	12.0(0.0)	1.7(0.0)	0.48	63.0(0.0)	15.0(0.0)	7.7(0.0)
16–15	59.4	7.73	60.3(0.1)	17.8(0.2)	146.2(1.5)	8.84	65.7(0.3)	22.1(0.8)	206.4(5.8)
16,1e–15,1e 3v7	1016.3	0.22	61.9(1.7)	10.0(0.0)	2.4(0.4)	0.65	65.5(1.6)	14.2(3.6)	9.87(2.1)
17–16	66.8	17.75	62.3(0.1)	14.9(0.2)	282.4(3.5)	11.20	64.2(0.1)	20.0(0.7)	240.1(6.2)
17,1f–16,1f 1v5	1021.1					1.24	63.3(0.4)	10.0(0.0)	13.2(0.7)
17,1f–16,1f 1v7	387.1	2.19	62.3(0.3)	15.7(0.6)	36.5(1.2)	3.99	64.7(0.3)	25.5(0.8)	108.3(3.0)
17,0–16,0 2v7	705.2	0.76	62.9(0.0)	12.0(0.0)	9.7(0.8)	1.56	71.9(0.6)	24.1(0.8)	40.1(0.8)
17,2e–16,2e 2v7	707.8	0.76	62.9(0.0)	12.0(0.0)	9.7(0.0)	1.56	71.9(0.0)	24.1(0.8)	40.1(0.0)
17,2f–16,2f 2v7	707.8	0.76	62.9(0.0)	12.0(0.0)	9.7(0.0)	1.56	71.9(0.0)	24.1(0.8)	40.1(0.0)
17,1e–16,1e 3v7	1023.7					1.0	62.6(1.4)	11.1(2.5)	11.8(2.7)
24,1e–23,1e 1v6	848.6	0.53	63.5(0.0)	11.0(0.0)	6.3(2.2)	1.59	78.7(2.1)	14.4(4.7)	24.3(0.8)
24,1e–23,1e 1v7	451.3	2.06	63.1(0.8)	17.0(0.0)	37.3(1.7)	5.89	66.9(0.8)	23.6(2.6)	147.8(0.8)
24,1f–23,1f 1v7	451.5	1.9	62.6(0.4)	18.8(0.8)	38.7(1.5)	5.54	65.9(0.1)	26.5(1.8)	156.6(0.9)

Table 4 lists the results of the Gaussian fits towards the new hot cores Sgr B2R1, Sgr B2R2, Sgr B2R3 and Sgr B2R4 determined from the 30m dish observations of the 10–9, 1v7,1f, 1v6,1e and 1v5,1f and 24–23,1v7,1f transitions. No ^{13}C isotope lines of HC_3N have been measured for these sources.

3.2. Interferometric data

Figs. 3a and 3b show the maps of the integrated intensity of the HC_3N J=10–9,1v7,1f line (at 64 kms^{-1}) towards Sgr B2M and Sgr B2N obtained with the PdB interferometer. The crosses show the location of the continuum peaks measured with the PdBI at 3 mm in both regions. The continuum flux densities are 3 Jy/beam for Sgr B2M and 2 Jy/beam for Sgr B2N. The HC_3N^* line emission is unresolved towards both hot cores with an upper limit to the size of the emitting regions of $3'' \times 5''$ (1/2 the HPBW). The peak of the HC_3N* emission is shifted from the continuum by $\sim 3''$ to the southeast for Sgr B2M and to the south for Sgr B2N. The condensations Sgr B2R1 and Sgr B2R2 are also seen at the border of the interferometric

Table 3. Fits for different $HC^{13}CCN$ (a) and $HCC^{13}CN$ (b) transitions towards Sgr B2M and Sgr B2N. Single dish observations

		Sgr B2M				Sgr B2N			
Transition	E_{upp} (K)	T_{mb} (K)	v ($km\,s^{-1}$)	Δv ($km\,s^{-1}$)	Area ($K\,km\,s^{-1}$)	T_{mb} (K)	v ($km\,s^{-1}$)	Δv ($km\,s^{-1}$)	Area ($K\,km\,s^{-1}$)
10,1e–9,1e 1v6	741.6	<0.01				0.19	60.1(0.4)	7.0(0.9)	1.5(0.1)
10,1f–9,1f 1v7	343.9	<0.03				0.25	63.5(1.4)	17.3(2.6)	4.6(0.4)
10,1e–9,1e 2v7	664.0	<0.01				0.12	64.9(1.2)	17.7(3.4)	2.4(0.2)
12,1f–11,1f 1v7	354.0	<0.07				0.21	62.9(1.5)	17.5(4.0)	3.9(0.5)
15–14	52.2	0.46	62.2(0.7)	15.1(1.8)	5.3(0.5)	1.13	65.5(1.2)	22.4(2.7)	26.9(3.6)
15–14	52.2	0.53	62.2(0.6)	13.8(1.3)	5.5(0.4)	0.98	68.1(1.6)	24.3(3.3)	25.3(3.6)
16–15	59.2	0.68	64.0(0.4)	13.5(0.9)	9.6(0.6)	1.03	67.5(0.6)	26.1(1.3)	28.7(1.4)
16–15	59.2	0.67	62.6(0.4)	13.4(0.9)	9.6(0.6)	1.10	65.6(0.4)	18.3(1.0)	21.4(1.2)
17–16	66.5	0.56	34.1(0.5)	17.6(1.6)	10.4(0.7)	1.14	65.9(1.3)	22.0(0.0)	26.6(1.2)
17–16	66.5	0.51	63.5(0.4)	15.2(1.0)	8.2(0.5)	0.98	63.4(0.9)	23.4(1.8)	24.6(1.8)
17,1f–16,1f 1v7	384.9	<0.07				1.03	65.3(0.5)	16.9(1.1)	18.7(0.7)

Table 4. Fits for different HC_3N vibrationally excited transitions towards Sgr B2R1, Sgr B2R2, Sgr B2R3 and Sgr B2R4. Single dish observations

Transition	T_{mb} (K)	v (K)	Δv ($km\,s^{-1}$)	Area ($K\,km\,s^{-1}$)
		Sgr B2R1		
10,1f–9,1f 1v5	0.06	67.4(2.0)	12.0(0.0)	0.84(0.3)
10,1e–9,1e 1v6	0.20	63.8(0.7)	11.7(1.7)	2.45(0.4)
10,1e–9,1f 1v7	0.43	65.5(0.4)	23.7(1.0)	11.04(0.5)
24,1f–23,1f 1v7	0.40	57.4(0.8)	7.5(2.3)	3.20(1.0)
		Sgr B2R2		
10,1f–9,1f 1v5	0.02	64.8(2.9)	17.0(0.0)	0.45(0.2)
10,1e–9,1e 1v6	0.10	63.9(1.0)	17.7(2.7)	1.90(0.3)
10,1f–9,1f 1v7	0.24	63.2(0.5)	19.1(1.5)	4.91(0.4)
24,1f–23,1f 1v7	0.28	59.6(0.4)	9.0(1.0)	2.70(0.2)
		Sgr B2R3		
10,1e–9,1e 1v6	0.11	65.3(1.1)	8.9(2.7)	1.07(0.4)
10,1f–9,1f 1v7	0.26	63.4(1.0)	14.0(0.0)	3.86(0.5)
24,1f–23,1f 1v7	0.24	62.4(0.7)	13.1(1.6)	5.01(0.5)
		Sgr B2R4		
10,1e–9,1e 1v6	0.12	65.3(0.8)	8.0(0.0)	1.03(0.2)
10,1f–9,1f 1v7	0.29	63.1(0.6)	17.2(1.9)	5.30(0.5)
24,1f–23,1f 1v7	0.34	58.8(0.8)	16.9(1.6)	6.06(0.6)

maps, although close to the noise limit (Fig. 3b). Fig. 4 shows the spectra taken towards the maximum of the HC_3N* emission in Sgr B2M (lower) and Sgr B2N (upper). We have used the main beam temperature as the intensity scale (conversion factor of 2.9 Jy/K).

Table 5 summarizes the results of the Gaussian fits performed to the HC_3N* profiles towards Sgr B2M and Sgr B2N. Lines towards Sgr B2N show two velocity components at 63 and 75 kms^{-1}. Each velocity corresponds to a different hot core, as we will see in Sect. 4. The line fluxes measured with the interferometer towards Sgr B2M and Sgr B2N are within the calibration errors (20%) of those obtained from single dish. Therefore, as expected, all the emission from HC_3N^* arises from compact sources unresolved with our resolution.

4. Velocity structure in the Sgr B2M and B2N cores

The gaussian fits obtained from single dish and interferometric observations show that the rotational lines arising from different vibrational levels have different line widths. The linewidth decreases as the energy of the vibrational level increases. In general, the 1v6 lines are narrower than the 1v7 lines by nearly a factor of 2 (see Table 6 for a summary). For Sgr B2N the lines are optically thick and opacity could explain some of the line broadening. However the $H^{13}CCCN$ lines in the 1v7 and 1v6 vibrationally excited states which are optically thin also show the same trend.

We can use the interferometric data to obtain more information about the velocity structure in the hot cores, when the interferometric data have high signal to noise ratio. We have determined the relative position of the line emission at different radial velocities within the synthesized beam by fitting the relative visibilities between the individual velocity channels. Fig. 5 shows the location of the HC_3N* J=10–9,1v7,1f emission at different radial velocities towards Sgr B2N and Sgr B2M superposed on the 1.3 cm continuum image from Gaume et al. (1995). We have also included in the same plot the position of H_2O masers (Reid et al., 1988; Kobayashi et al., 1989), the NH_3 (Vogel et al., 1987) and CH_3OH cores (Mehringer & Menten, 1997) and our 3.3 mm peak continuum emission. Fig. 6 shows an average position-velocity plot for Sgr B2N. The data were obtained averaging the velocity channels for transitions HC_3N* 10–9,1v7,1f, 1v7,1e6, 1v6,1e and 1v5,1f weighted with their error.

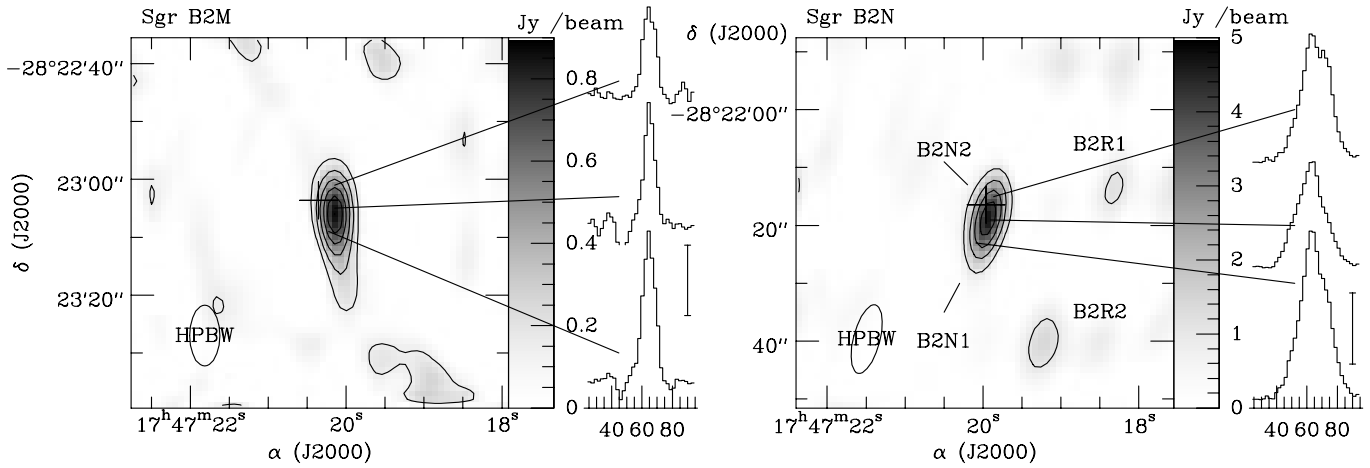

Fig. 3a and b. Line emission from transition HC_3N* 10-9,1v7,1f towards Sgr B2M and Sgr B2N as observed with the Plateau de Bure Interferometer. The cross represents the continuum position at 91 GHz. Sgr B2M: levels at 0.14, 0.29, 0.43, 0.58, 0.72 and 0.87 Jy/beam. Sgr B2N: levels at 1.2, 2.3, 3.4 and 4.5 Jy/beam. The vertical bar accompanying the spectra represents an intensity of 0.5 Jy/beam in Sgr B2M and 2 Jy/beam in Sgr B2N.

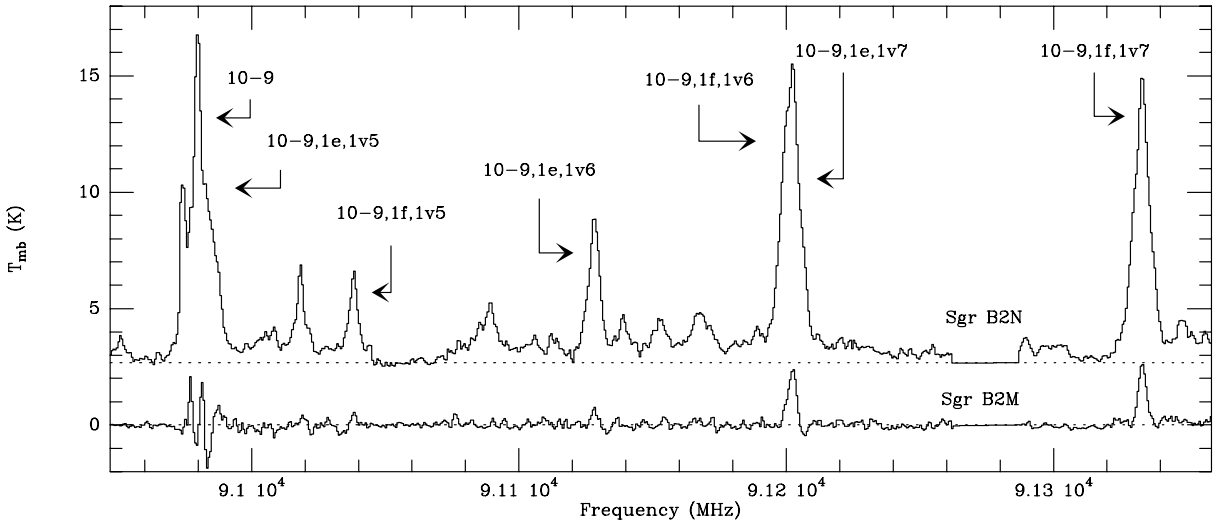

Fig. 4. Spectra of the HC_3N* lines towards Sgr B2M (lower) and Sgr B2N (upper) as obtained with the Plateau de Bure Interferometer.

4.1. Sgr B2N

The hot gas in Sgr B2N shows a systematic trend in the position of the HC_3N* emission as the radial velocity changes. For velocity ranges between 50 and 70 kms^{-1} the emission at lower velocities occurs towards the east and for higher velocities towards the west. For radial velocities between 70-80 kms^{-1}, the HC_3N emission shifts abruptly $2''$ to the north (see also Fig. 3, Fig. 6) This shift suggests that the emission between 70 and 80 kms^{-1} comes from a different hot core than the HC_3N emission at 60-70 kms^{-1}. A similar suggestion has also been made by Miao et al. (1995) and Liu & Snyder (1999) from C_2H_5CN line observations. However these authors estimate a distance of $5''$ between both peaks.

Other evidence for the presence of recent massive star formation near to the hot core at 70-80 kms^{-1} comes from the detection of UC HII region K3 with a radial velocity of 71 kms^{-1} (de Pree et al., 1995). Furthermore Lis et al. (1993) detected extended dust emission in the north-south direction, which indicates the presence of two dust condensations. Therefore the final picture for Sgr B2N, supported by all data, suggests that it is composed by two hot cores, one at 60 kms^{-1} (Sgr B2N1) and the other at 75 kms^{-1} (Sgr B2N2) separated $2''$ in a south-north direction.

4.2. Sgr B2M

HC_3N emission towards Sgr B2M also shows some kinematic structure although the larger errors make this determination very uncertain. Radial velocities increase for decreasing RA. The same trend is observed in the H_2O maser emission (Kobayashi et al., 1989). Other molecular tracers show different behavior as a function of radial velocity. Vogel et al. (1987) the NH_3 emission found from the NH_3 emission that the blue-

Table 5. Fits for different HC_3N vibrationally excited transitions towards Sgr B2M and Sgr B2N. Interferometric observations

		Sgr B2M				Sgr B2N			
Transition	E_{upp} (K)	T_{mb} (K)	v (km s^{-1})	Δv (km s^{-1})	Area (K km s^{-1})	T_{mb} (K)	v (km s^{-1})	Δv (km s^{-1})	Area (K km s^{-1})
10,1f–9,1f 1v5	978.3	0.52	65.2(0.4)	6.6(1.2)	3.7(0.6)	3.55	63.9(0.1)	10.7(0.1)	40.6(0.5)
						0.41	75.0(0.0)	5.0(0.8)	2.2(0.4)
10,1e–9,1e 1v6	741.3	0.73	64.9(0.6)	8.2(1.2)	6.4(0.9)	6.12	62.8(0.2)	14.9(0.5)	97.5(2.8)
						1.11	75.6(0.6)	6.4(0.9)	7.6(2.1)
10,1f–9,1f 1v6	741.3	0.69	65.4(0.3)	6.8(1.6)	5.2(0.9)	1.60	69.3(0.9)	16.0(0.0)	27.0(1.5)
10,1e–9,1e 1v7	344.1	2.51	65.4(0.3)	10.3(0.0)	27.4(0.9)	10.77	64.6(0.2)	23.0(0.0)	262.7(1.4)
10,1e–9,1f 1v7	344.1	2.48	65.1(0.2)	10.9(0.4)	28.8(0.9)	11.91	62.2(0.2)	17.0(0.0)	215.6(4.4)
						4.51	75.0(0.0)	15.2(1.1)	73.0(5.8)

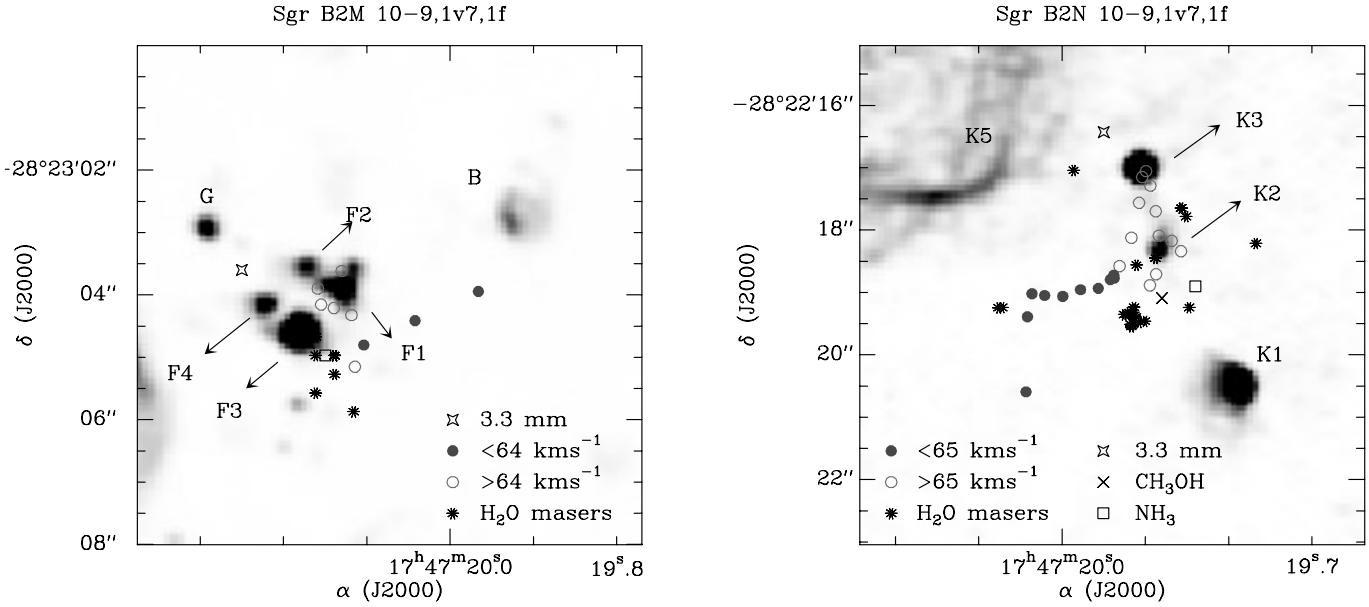

Fig. 5. Location of the HC_3N* 10–9,1v7,1f velocity features (circles) towards Sgr B2N and Sgr B2M, as obtained from the interferometer using an UV fitting technique. Circles are plotted in steps of 2.1 kms^{-1}. The background image is the 1.3 cm continuum image from Gaume et al. (1995). Asterisks correspond to H_2O maser positions from Reid et al. (1988) (Sgr B2N) and Kobayashi et al. (1989) (Sgr B2M), diamonds to 3.3 mm peak emission (this article), squares to NH_3 thermal cores (Vogel et al., 1987), and crosses to CH_3OH thermal cores (Mehringer & Menten, 1997)

shifted and red-shifted components are separated. Gaume & Claussen (1990), with higher angular resolution observations of NH_3, see a continuous north-south velocity gradient. Lis et al. (1993) point out that the velocity gradient obtained from HC_3N 25–24 emission in the SE-NW direction does not agree with the structure seen in NH_3 and suggest that HC_3N and ammonia may be tracing different components.

5. Location of the emission regions

Table 7 summarizes the location of the 3.4 mm continuum and the HC_3N* line peak emission as derived from Gaussian fits to the integrated intensity of the different HC_3N^* lines. For comparison we have also included the positions of the H_2O masers (Reid et al., 1988), the NH_3 (Vogel et al., 1987) and CH_3OH (Mehringer & Menten, 1997) thermal cores, our 3.3 mm, the 3.4 mm (Carlstrom & Vogel, 1989) and 1.3 mm continuum peak emission (Lis et al., 1993), and the nearest ultra-compact HII (UC HII) regions, K2, K3 and F2 measured at 1.3 cm (Gaume et al., 1995). The position in Table 7 for the H_2O maser

Table 6. Line widths averaged for different HC_3N vibrationally excited transitions towards Sgr B2M and Sgr B2N. Single dish observations

	Sgr B2M		Sgr B2N	
	^{12}C	^{13}C	^{12}C	^{13}C
Transition	Δv (km s^{-1})	Δv (km s^{-1})	Δv (km s^{-1})	Δv (km s^{-1})
v0	17.4(0.8)	14.3(0.4)	21.6(0.7)	21.8(1.7)
v7	16.2(1.0)		25.5(1.1)	17.0(1.0)
2v7	12.0(1.0)		21.8(2.8)	17.7(3.4)
v6	10.8(0.7)		16.6(0.9)	7.0(0.9)
3v7	9.5(0.5)		13.3(0.9)	
v5	9.6(2.3)		13.8(0.9)	

Table 7. Location of the emission regions for the mm continuum, some HC_3N* 10–9 transitions, and other tracers towards Sgr B2M and Sgr B2N.

	Sgr B2M		Sgr B2N	
Transition	α (J2000) $17^h\ 47^m$	δ (J2000) $-28^o\ 23^m$	α (J2000) $17^h\ 47^m$	δ (J2000) $-28^o\ 22^m$
HC_3N 1v7,1f	20.15 ± 0.04	03.20 ± 0.5	19.94 ± 0.01	18.64 ± 0.4
HC_3N 1v7,1e	20.15 ± 0.04	04.20 ± 0.5	19.94 ± 0.5	18.86 ± 1
HC_3N 1v6,1e	20.15 ± 0.07	05.20 ± 1.0	19.94 ± 0.5	18.86 ± 1
HC_3N 1v5,1e	20.15 ± 0.11	05.50 ± 2.0	19.94 ± 0.5	18.76 ± 1
3.3mm Cont.	20.25	03.60	19.95	16.43
3.4mm Cont. [1]	20.17 ± 0.02	04.77 ± 0.5	19.87 ± 0.02	18.79 ± 0.5
1.3mm Cont. [2]	20.16	04.97	19.89	17.79
H_2O [3,4]	20.13 ± 0.003	04.30 ± 0.06	19.91 ± 0.003	19.47 ± 0.06
NH_3 [5]	20.17	04.77	19.88	19.09
CH_3OH [6,7]	20.15 ± 0.05	04.97 ± 0.7	19.84 ± 0.05	18.90 ± 0.7
UC HII region [8]	20.17 ± 0.01	03.57 ± 0.1	19.88 ± 0.01	18.39 ± 0.1

[1] Carlstrom & Vogel (1989), [2] Lis et al. (1993), [3] Kobayashi et al. (1989)
[4] Reid et al. (1988), [5] VGP (1987), [6] Mehringer & Menten (1997)
[7] Houghton & Whiteoak (1995), [8] Gaume et al. (1995): F2(B2M), K2 & K3(B2N)

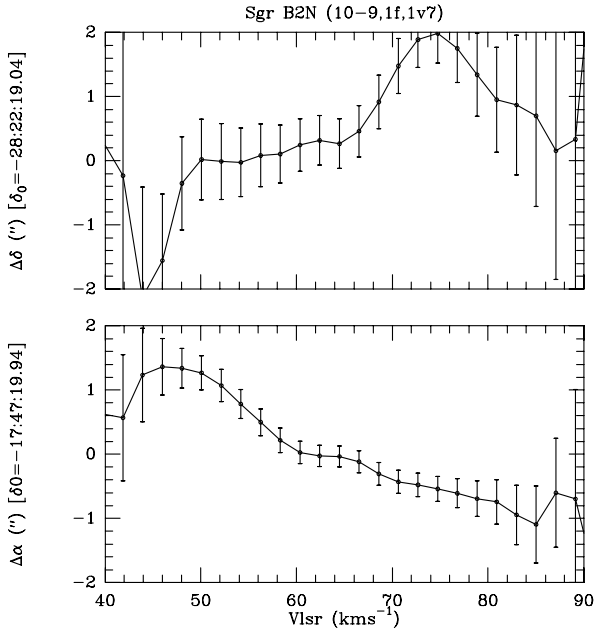

Fig. 6. 10–9,1f,1v7 spatial position in RA and DEC for each velocity channel as obtained from a fitting process (see Sect. 4).

emission (Reid et al., 1988) corresponds to the cluster with the largest number of features (12).

The position for other masers such as H_2CO (Mehringer et al., 1995), OH (Gaume & Claussen, 1990) and CH_3OH (Mehringer & Menten, 1997) detected towards Sgr B2N and Sgr B2M have not been included in Table 7 because they do not come from the same region where the HC_3N* lines arise and apparently do not have relation with these cores. They are probably related to the hot expanding shells discovered by Martín-Pintado et al. (1999).

As already stated in Sect. 3.2, the positions of the 3.3 mm continuum peak are different from the HC_3N* peak emissions, indicating that the hot cores observed in HC_3N are located in different regions than the HII regions. Our continuum maxima at 3.3 mm also differ from the 3.4 mm maxima (Carlstrom & Vogel, 1989) by $\sim 1.5''$ and $1''$ in Sgr B2N and Sgr B2M, which is probably due to the complex distribution of HII regions in both sources and the different beam sizes. The HC_3N positions in Sgr B2M and Sgr B2N agree within $1''$ with the positions of the H_2O masers in each source, indicating that the two emissions must be related. Furthermore the HC_3N* emission also peaks close to the CH_3OH and NH_3 thermal cores and therefore the two emissions are likely associated.

The IR radiation, which is the main excitation mechanism for HC_3N*, might also be responsible for the pumping of the H_2O masers. The lack of radiocontinuum emission associated with the hot cores suggests that these IR sources have not yet ionized their surroundings.

None of the Sgr B2R hot cores is coincident with any HII region (Gaume et al., 1995). Sgr B2R1 is $10''$ southeast of UC HII region X8.33, Sgr B2R2 is $3''$ north of UC HII region Z10.24, while Sgr B2R3 is $5''$ south of it. Sgr B2R4 is within $1''$ distance of HII region A1. The Sgr B2W extended emission encompasses HII regions A2, A1, B9.89, B9.99, B9.96, Y, E, D and C (Gaume et al., 1995). None of the Sgr B2R cores coincides with the 6.7 GHz methanol masers (Houghton & Whiteoak, 1995) although they are within a distance of $10''$ of some of them. Sgr B2R2 and Sgr B2R4 are $2''$ from two H_2O maser features (Kobayashi et al., 1989). As for the Sgr B2M and Sgr B2N hot cores, the Sgr B2R hot cores have not yet evolved to the UC HII region stage.

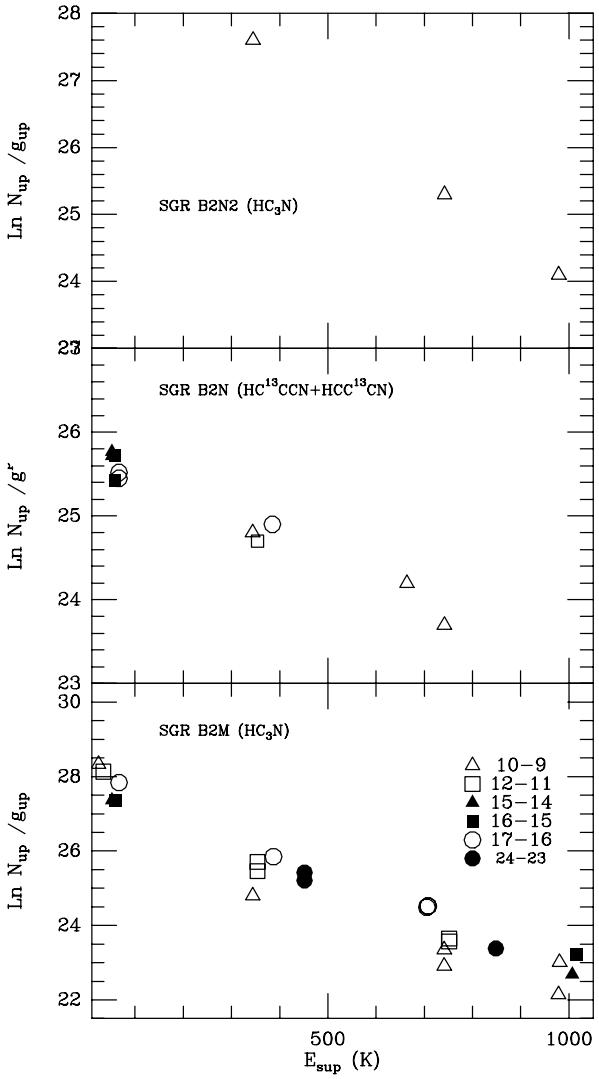

Fig. 7. Population diagram of vibrationally excited transitions. From single dish observations towards Sgr B2M and Sgr B2N1 and from interferometric observations towards Sgr B2N2.

6. Properties of the hot cores determined from HC_3N*

The HC_3N* lines observed in this paper sample hot gas in a wide range of temperatures from the ground state up to 1000 K. Combining the emission from all lines one can study the density and the temperature gradients in the hot cores. Table 8 summarizes the main physical parameters (excitation, temperature, HC_3N column density, sizes and abundance) for the hot cores as derived from the HC_3N* data presented in this paper.

6.1. Excitation temperatures and HC_3N column densities

From the single dish optically thin HC_3N* lines towards Sgr B2M and the ^{13}C isotopic substitution of HC_3N* lines towards Sgr B2N1 we have determined the HC_3N column densities in different vibrational levels for both hot cores. We have also used the interferometric HC_3N* lines at 75 kms^{-1} to estimate the HC_3N column densities in the different vibrational levels towards Sgr B2N2. The column densities for Sgr B2N2 are uncertain because of the blending with the Sgr B2N1 lines and should be considered as rough guidelines.

Fig. 7 shows the population diagram (see Goldsmith & Langer (1999) for an explanation of the nomenclature) for Sgr B2M, Sgr B2N1 and Sgr B2N2. Surprisingly, a straight line can fit all the data points for all sources. The slope of this line should be related to the excitation temperature. We estimate excitation temperatures of $\sim$190 K towards Sgr B2M, $\sim$350 K from the $HC^{13}CCN$ and $HCC^{13}CN$ data towards Sgr B2N1 and $\sim$180 K towards Sgr B2N2. The excitation temperatures that we obtain towards Sgr B2M and Sgr B2N1 are in good agreement with those determined from the ground states lines of CH_3CN by de Vicente et al. (1997) and from NH_3 towards Sgr B2M by Vogel et al. (1987).

However, as mentioned in Sect. 4, the linewidths for the different vibrational transitions are different with the width of the lines decreasing as the energy of the vibrational levels increases. Therefore, the excitation temperature derived from the population diagrams does not reflect the actual temperature structure of the hot cores. If we use the linewidth of the 1v5,1f for Sgr B2M and Sgr B2N1, and the linewidth of 1v6,1e for Sgr B2N2, we obtain excitation temperatures of $\sim$350 K for Sgr B2M, $\sim$700 K for Sgr B2N1 and $\sim$270 K for Sgr B2N2. This behaviour clearly indicates that the excitation temperature in the hot core has a gradient as a function of the distance to the heating source. This will be discussed in detail in the model presented in Sect. 7.

The beam averaged HC_3N column density obtained using excitation temperatures of 190 K towards Sgr B2M, 350 K towards Sgr B2N1 and 180 K towards Sgr B2N2, is $2\,10^{15}$ cm^{-2} for Sgr B2M, 10^{16} cm^{-2} towards Sgr B2N1 and $7\,10^{15}$ cm^{-2} towards Sgr B2N2. To obtain the total column densities we have computed the partition function including all vibrational levels with energies up to 1100 K, and assuming LTE population with the excitation temperature derived from the rotational diagrams and a $^{12}C/^{13}C$ ratio of 20.

The excitation temperatures of the hot cores Sgr B2R1, B2R2, B2R3 and B2R4 have been estimated from the J=10–9 1v5,1f, 1v6,1e and 1v7,1f column densities measured with the 30m dish. In case that opacity effects are important in these lines the estimated excitation temperatures and column densities are lower limits to the actual values. The estimated excitation temperatures are 270, 320, 240 and 250 K and the beam averaged HC_3N total column densities 10^{15}, $7\,10^{14}$, $5\,10^{14}$ and $6\,10^{14}$ cm^{-2} for Sgr B2R1, B2R2, B2R3 and B2R4 respectively.

6.2. Size of the emitting regions

The interferometric maps show that the HC_3N* emission towards Sgr B2N and Sgr B2M is unresolved, and therefore we can place an upper limit of $3'' \times 5''$ to the size of the hot cores, which is consistent with the size of the emission presented in Fig. 5. We can also use brightness temperature arguments to estimate the area of the emitting region when its corresponding size (θ_s) is smaller than the beam (θ_b). For this, we will use the line intensity at the radial velocity where the line peaks. A lower

Table 8. Hot core properties.

Hot Core	α (J2000) 17^h47^m	δ (J2000) -28^h 23^m	N(HC_3N) [b] (cm^{-2})	T_{ex} (K)	Size ($''$) (Lower)	(Upper)	n(H_2)[b] (cm^{-3})	N(H_2)[a] (cm^{-2})	X(HC_3N)[b]	Mass[b] ($M_\odot$)	L[b] ($L_\odot$)
Sgr B2M	20.15	04.00	$7\,10^{16}$	190	1.8×1.8^d	3×5	$5\,10^7$	$1.4\,10^{25}$	$5\,10^{-9}$	500	$3\,10^6$
Sgr B2N1	19.94	18.74	10^{18}	350	0.5×0.5	3×5	$6\,10^7$	10^{25}	10^{-7}	200[c]	$2\,10^7$
Sgr B2N2	19.90	17.30	$9\,10^{16}$	180	0.5×0.5	3×5	$2\,10^8$	$3\,10^{25}$	$3\,10^{-9}$	600[c]	$3.4\,10^6$
Sgr B2R1	18.64	18.74	$5\,10^{17}$	270	0.7×0.7	7×7	$<10^7$	$<2.5\,10^{24}$	$>2\,10^{-7}$	<10	$3\,10^6$
Sgr B2R2	20.00	38.00	$7\,10^{17}$	320	0.6×0.6	7×7	$3\,10^7$	$3\,10^{24}$	$2\,10^{-7}$	30	$5\,10^6$
Sgr B2R3	20.00	50.00	$2\,10^{17}$	240	1.0×1.0	7×7	$<10^7$	$<10^{24}$	$>2\,10^{-7}$	<10	$2\,10^6$
Sgr B2R4	19.38	00.40	$2\,10^{17}$	250	0.8×0.8	7×7	$<10^7$	$<10^{24}$	$>2\,10^{-7}$	<10	$3\,10^6$

[a] Estimated from interferometric 1.3mm flux measurements by Lis et al. (1993).
[b] Calculated assuming $\theta_s = 2''$ for SgrB2M and $\theta_s = 1.5''$ for Sgr B2N1 and B2N2 and $\theta_s = 1.5''$ for Sgr B2R1 to B2R4.
[c] The total mass for the Sgr B2N core is ~ 800 $M_\odot$
[d] Size estimated only for the 1v7,1f and 1v7,1e emission.

Table 9. HC_3N* core sizes towards Sgr B2N estimated from a line opacity of 4.5

Transition	Size (arcsec)
10–9,1v7,1f	$1.5''\times1.5''$
10–9,1v6,1e	$1.0''\times1.0''$
10–9,1v5,1f	$0.8''\times0.8''$
10–9,2v7,1f	$0.5''\times0.5''$
10–9,3v7,1f	$0.7''\times0.7''$

limit to the area of the source, assuming circular geometry, is given by, $\theta_s^2 \geq \theta_b^2 T_{mb}/T_b$, where T_b is the brightness temperature of the emission and T_{mb} is the main beam temperature. In the case of Sgr B2N1 the HC_3N* lines of the main isotope are optically thick and therefore the brightness temperature must equal the excitation temperature. Using the excitation temperature derived from the population diagrams ($\sim$ 350 K) and a line opacity of 4.5 (derived in Sect. 3.1)for all transitions, we obtain the source sizes summarized in Table 9. Columns 6 and 7 of Table 8 give the upper and lower limits to the actual source sizes. Size limits for Sgr B2N1 are consistent with the extent of this hot core as derived from kinematic data. If the lines are optically thick, the actual area of the hot cores in the sky for the different HC_3N* lines must be close to those in Table 8.

The source size is different for the various HC_3N* transitions towards Sgr B2N1, indicating the presence of a temperature gradient. In this case the derived excitation temperature from the population diagrams ($\sim$ 350 K) must be considered a mean dust temperature in the hot core.

The size of Sgr B2N2 is difficult to estimate since we ignore the opacity of these lines. However from Fig. 5 we may accept $1.5''$ as a reasonable value.

The opacities of the HC_3N* lines towards Sgr B2M are small and therefore we can only give a lower limit to the size of the core. The value shown in Table 8, $1.8''\times1.8''$, has been obtained from the J=17–16,1v7,1f transition assuming that the line is optically thick and an excitation temperature of 190 K. The upper limit size in Table 8 is derived from our beam (1/2 HPBW). Sizes of the Sgr B2M and Sgr B2N hot cores have also been measured from interferometric data, such as continuum (Lis et al., 1993), NH_3 emission (Vogel et al., 1987) and thermal CH_3OH emission (Mehringer & Menten, 1997). These sizes are slightly larger or similar to those derived in this section. Sizes of the Sgr B2R1 to B2R4 cores are difficult to estimate. We can set a lower limit using the same arguments as for Sgr B2N for the J=24–23,3v7,1f transition. The results are summarized in Table 8.

6.3. HC_3N abundance, H_2 density and masses

The HC_3N abundance in Sgr B2M, Sgr B2N1 and Sgr B2N2 can be inferred from our HC_3N column densities and the H_2 column density estimated by Lis et al. (1993) from continuum measurements at 1.3 mm obtained with similar angular resolution. Since the HC_3N source sizes for the Sgr B2M, Sgr B2N1 and Sgr B2N2 hot cores are 1-2$''$, one order of magnitude smaller than the smallest single dish beam used in our observations, the beam averaged HC_3N column density derived in Sect. 4.1 must be corrected for beam dilution effects. This increases the HC_3N column density by approximately two orders of magnitude for the single dish data and one order of magnitude for the interferometric data. The corrected HC_3N column densities for all hot cores are given in Column 4 of Table 8.

We have recalculated the H_2 column densities from the continuum measurements of Lis et al. (1993). We have assumed that the dust temperatures are similar to the HC_3N* excitation temperatures, a dust emissivity with a power law with a slope of 1.1 for all sources (see Martín-Pintado et al. (1990) and Lis et al. (1993) for a discussion on this issue), and the peak flux densities measured by Lis et al. (1993), with the free-free contribution subtracted.

Lis et al. (1993) report a deconvolved size for the dust emission towards Sgr B2N of $<1.3''\times5''$ in the south-north direction. The size of the hot core determined from the HC_3N* emission, $1.5''$, is similar to the size of the dust in RA. As discussed in Sect. 4 the elongation in declination of the dust emission is due to two hot cores with sizes of $\sim 1.5''$ separated by $2''$. We

have considered half the total continuum flux at 1.3mm to be associated with each hot core (9 Jy/beam).

Under the previous hypothesis we obtain mean H_2 column densities of $1.4\,10^{25}$ cm^{-2} towards Sgr B2M and 10^{25} cm^{-2} towards Sgr B2N1 and $3\,10^{25}$ cm^{-2} towards Sgr B2N2 (see Table 8). The H_2 column density for Sgr B2R2 has been estimated from the continuum interferometric flux measured by Lis et al. (1993), assuming a source size of 1 arcsec, a temperature of 350 K and a flux of 1 Jy/beam. Towards Sgr B2R2 we get an H_2 column density of $3\,10^{24}$ cm^{-2}.

For the total HC_3N column densities of $7\,10^{16}$ cm^{-2} for Sgr B2M, 10^{18} cm^{-2} for Sgr B2N1, $9\,10^{16}$ cm^{-2} for Sgr B2N2 and $7\,10^{17}$ for Sgr B2R2 and the H_2 calculated densities, we determine a fractional HC_3N abundance of $5\,10^{-9}$, 10^{-7}, $3\,10^{-9}$ and $2\,10^{-7}$ towards Sgr B2M, Sgr B2N1, Sgr B2N2 and Sgr B2R2 respectively.

For the other hot cores in the ridge we can only set lower limits to the HC_3N abundance considering the upper limit to the continuum flux density at 1.3mm and assuming a typical size for the hot cores of $1''$. We estimate a lower limit to the HC_3N abundance of $2\,10^{-7}$, in agreement with that obtained for the Sgr B2R2 hot core. Lower abundances of HC_3N are possible only if the hot cores Sgr B2R1, B2R3 and B2R4 are substantially larger.

For a depth along the line of sight similar to the size of the hot cores we estimate mean H_2 densities of $7\,10^7$ cm^{-3} for Sgr B2M and $6\,10^7$ cm^{-3} for Sgr B2N1, $2\,10^8$ cm^{-3} for Sgr B2N2 and $3\,10^7$cm^{-3} for Sgr B2R2. Assuming a spherical geometry, and the previous densities we derive masses of 500 $M_\odot$ for Sgr B2M and 200 $M_\odot$ for Sgr B2N1, and 600 $M_\odot$ for Sgr B2N2. Then the total mass in Sgr B2N would be roughly $\sim$ 800 $M_\odot$, similar to that in Sgr B2M. The masses for the ridge hot cores are between 10 to 30 $M_\odot$, substantially smaller than those for Sgr B2M and Sgr B2N (see Table 8).

6.4. Luminosities

The high temperatures obtained from the HC_3N* emission indicate that the hot cores are internally heated. For the derived H_2 densities (10^7–10^8 cm^{-3}) gas and dust are coupled and the excitation temperature given in Table 8 should also correspond to the dust temperature.

For the H_2 column densities derived previously, the dust is optically thick even at 100 μm, indicating that the hot cores emit like a blackbody at the dust temperature. The bolometric luminosity of the hot cores can be estimated from the Stefan-Boltzmann law. The results, obtained assuming a source radius of $1''$ for Sgr B2M, $0.75''$ for Sgr B2N1 and Sgr B2N2 and $0.5''$ for Sgr B2R1 to B2R4, are summarized in Table 8.

The luminosity may be overestimated due to geometric effects (the sources may have a disk geometry instead of a spherical one, see Cesaroni et al. (1997)). However lower luminosities would not explain the sizes of the HC_3N* emission lines (see next section).

7. The distribution of the hot dust in the hot cores

Goldsmith et al. (1985b) argued, based on the thermalization at only one temperature and on the large H_2 densities (10^{10} cm^{-3}) required for the collisional excitation of the HC_3N* lines, that these lines are excited by IR radiation. Similar arguments also apply to the Sgr B2 hot cores. The HC_3N* rotational lines from different vibrational levels will trace IR emission at the wavelength of the vibrational transitions. One can then use the different sizes obtained from the lines to study the thermal structure of the dust and gas surrounding the young massive stars.

In order to understand the population diagrams derived from the HC_3N* data we have developed a simple model to study the excitation of the HC_3N* emission for a condensation of gas and dust surrounding a young star. For simplicity, we have considered that the hot cores have spherical geometry with an inner radius of 10^{16} cm. The excitation temperature of the HC_3N* lines (1v7, 1v6, 1v5, 2v7 and 3v7) has been assumed to be equal to the dust temperature as expected from H_2 densities of $> 10^6$ cm^{-3} derived for the hot cores in Sgr B2. For the H_2 column densities we derive for the hot cores (Table 8), the dust emission at the wavelenghts where the vibrational excitation of HC_3N ocurrs is optically thick. In this case, one can consider that dust and gas are coupled and that the radial profile of the dust temperature can be approximated by the Stefan-Boltzmann law:

$$T_{dust} = \left(\frac{L_\star}{4\pi\sigma r^2}\right)^{1/4} = 15.222\left(\frac{L_\star}{L_\odot}\left[\frac{10^{16}\mathrm{cm}}{r}\right]^2\right)^{1/4} \quad (1)$$

This approximation gives a similar dust temperature profile to that obtained by Lis & Goldsmith (1990) from models that solve the radiative transfer in a dusty cloud for the distances from the heating source relevant to our model, between $3\,10^{16}$ cm and $3\,10^{18}$ cm. The main discrepancies between the temperatures from expression 1 and the radial profile from Lis & Goldsmith (1990), are found in a very small region (10^{16} to $3\,10^{16}$ cm) around the star which has a negligible contribution to the HC_3N* line intensities.

To perform the radiative transfer in the cloud we have divided the hot core into 300 shells. The H_2 density has been considered to decrease with the distance as $r^{-3/2}$ as expected for a hot core (Osorio et al., 1999). We have also considered a constant HC_3N abundance through the hot core. The widths of the HC_3N* lines used in the model were 6 and 10 kms^{-1} for Sgr B2M and Sgr B2N1 respectively.

Table 10 shows the parameters for Sgr B2M and Sgr B2N1 that give the best fit to the HC_3N* data. Fig. 8 shows the model predictions in the form of population diagrams. To compare the results of the model (filled circles) with our data we also show in Fig. 8 a comparison with the population diagrams derived from the data obtained with the interferometer (open circles). It is interesting to note that, in spite of the presence of a temperature gradient within the hot core, as expected for excitation by radiation, the population diagrams shows a straight line indicating a single excitation temperature.

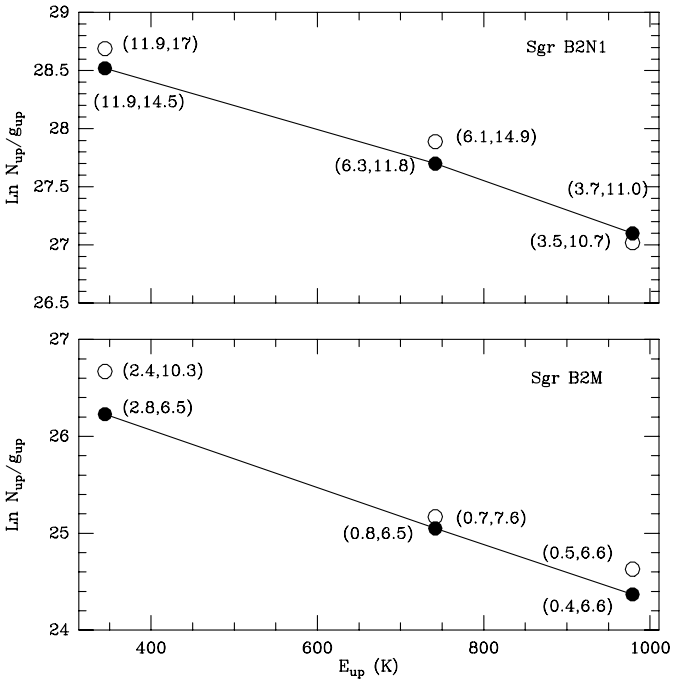

Fig. 8. Population diagrams comparing the interferometric data (open circles) and the results from the model for transitions 10–9 1v7,1f, 1v6,1e and 1v5,1f (filled circles). Numbers between parenthesis indicate i T_{mb} (K) and line width (kms^{-1} respectively for each transition.

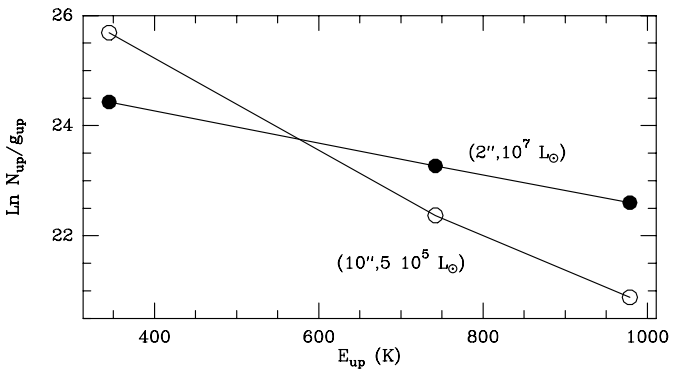

Fig. 9. Population diagram obtained from the model described in Sect. 7, comparing a source of a size of $2''$ with a luminosity of 10^7 $L_\odot$, (filled circles), with source of a size of $10''$, with a luminosity of $5\,10^5$ $L_\odot$ (open circles). The points correspond to transitions 10–9, 1v7,1f, 1v6,1e and 1v5,1f.

Table 10. Final parameters used in the model.

Parameter	Sgr B2M	Sgr B2N1
Luminosity ($L_\odot$)	$2\,10^7$	10^7
Distance (pc)	7100	7100
n(H_2) (cm^{-3}, $r_0 = 10^{16}$ cm)	$6\,10^8(r/r_0)^{-3/2}$	$10^9(r/r_0)^{-3/2}$
HC_3N line width (kms^{-1})	6.5	10
HC_3N abundance	$5\,10^{-9}$	10^{-7}
Source size (arcsec)	3	1.9

Although the sizes of the hot cores have been estimated from the HC_3N* line intensities we have considered both the sizes and the luminosities as free parameters. One interesting result from our modelling is that the shape of the population diagrams depends on the size and the luminosity of the hot core. Fig. 9 shows the population diagrams for a hot core with a size of $2''$ as measured for Sgr B2N1 with the estimated luminosity of 10^7 $L_\odot$ and a hot core with the size of $10''$ and a luminosity of $5\,10^5$ $L_\odot$. The population diagram predicted for the large hot core with low luminosity shows the typical shape of a temperature gradient and cannot be fitted by a straight line. On the other hand, one obtains the population diagram that can be fitted by a straight line if the size of the hot core is relatively small and the luminosity high. This is because for the latter case the range of dust temperatures within the hot cores is relatively small; the range of temperatures that contribute to the HC_3N* emission is between 200 and 330 K (radii between $1.8\,10^{17}$ and $7\,10^{16}$ cm). Under this condition the population diagrams will be represented by a straight line with an excitation temperature close to the average temperature in the hot core. This indicates that the HC_3N* emission should be restricted to a smaller region to that expected to be excited in the 1v7 line. The small size of the HC_3N* hot core could be due to a sharp drop of the HC_3N abundance or of the H_2 densities. The first possibility is the most likely since the large HC_3N abundances (see Sect. 8) requires a particular chemistry (HC_3N evaporation from grains) which is strongly coupled to the temperature.

The main results obtained from the model can be summarized as follows:

- The observed line intensities (values in parenthesis in Fig. 8) towards Sgr B2N1 and Sgr B2M are fitted by the model within 20%. The discrepancies, between the model predictions and the data in the population diagrams are due to the different line width of the observed lines.
- The model predicts that the lines towards Sgr B2N1 are broadened by opacity. However the opacity cannot reproduce the observed large linewidth for the 1v7 and 1v6 transitions. This is consistent with the $HC^{13}CCN$* data and indicates the presence of systematic kinematic effects within the hot core.
- The luminosity needed to fit the line intensities towards Sgr B2M is higher than that estimated in Sect. 6.4 by a factor of $\sim$10. If we use the luminosity in Table 8, the observed T_{mb} ratios between 1v7, 1v6 and 1v5 transitions cannot be reproduced.

8. Hot core chemistry

One of the most remarkable results from our data is the large abundance of HC_3N towards the hot cores in Sgr B2, specially towards Sgr B2N1 and Sgr B2R1 to B2R4, where it is of the order of 10^{-7}. Typically, HC_3N emission is found in warm clouds like the extended ridge and fingers in Orion A (Rodríguez-Franco et al., 1998) where its abundance is 10^{-9}. In Orion A, the HC_3N abundance increases by one order of magnitude (10^{-8}) for the hot core and decreases one order of magnitude towards the photo-dissociation regions in the ioniza-

tion fronts of the HII region Orion A. In fact, Rodríguez-Franco et al. (1998) propose that the large abundance of HC_3N emission is a good tracer of hot cores and regions which are well shielded from the UV radiation. The HC_3N abundance we estimate for Sgr B2N1 and Sgr B2R1-B2R4 agrees with the maximum abundance in the gas phase that Caselli et al. (1993) obtain, at a time of $\sim 3\,10^4$ yr, after the startup of gravitational collapse for an Orion hot core type. Caselli et al. (1993) developed a model that considers the evolution of the chemistry of some molecules in the formation of a massive star. The HC_3N abundance towards Sgr B2M is better fit by the abundance values obtained for the hot core phase, when accretion has stalled and molecules are evaporated from grains.

The large difference in the HC_3N abundance between Sgr B2M and Sgr B2N1 could also be related to the UV radiation from nearby OB stars that penetrates deeper in the hot core and photodissociate the fragile molecules like HC_3N. Indeed the Sgr B2M complex has more than 20 HII regions powered by OB stars within $5''$ from the Sgr B2M hot core (Gaume et al., 1995) which should produce an intense UV radiation field. This contrasts with Sgr B2N, where there are fewer HII regions. The same explanation applies to the Sgr B2R cores, where the abundance is similar to that in Sgr B2N and where there is one or no HII regions in the neighborhood of the hot core. The low HC_3N abundance towards Sgr B2N2 has no simple explanation.

9. Kinematics of the Sgr BM and Sgr B2N hot cores

One of the most remarkable results of the observations of HC_3N* towards the hot cores is the decrease of the linewidth as the energy of the vibrational level in which the rotational lines arise increases. This systematic trend in the linewidth combined with different sizes of the region where the different vibrationally excited lines arise indicates that the linewidth of the HC_3N* lines depends on the distance to the exciting source. There are two possibilities to explain the larger line widths for the larger distances.

The first possibility is that the HC_3N* linewidth is dominated by turbulence, with the linewidth depending on the size of the eddies. The second possibility is that the velocity systematically increases with the distance to the source. This is the most likely explanation in view of the previous kinematical results on both sources. We discuss now the implications of the results presented in this paper on the kinematics of the hot cores in Sgr B2M and Sgr B2N.

9.1. Sgr B2N

The kinematics in the Sgr B2N hot core has been subject of debate. Lis et al. (1993), from the map of the J=25–24 HC_3N line, and de Vicente (1994), based on the spatial distribution of the high velocity gas observed in the J=13–12 and J=20–19 OCS rotational lines, proposed an east-west outflow. Reid et al. (1988) suggested from a model to fit the proper motion of the H_2O masers, that the kinematics is due to a solid body rotation in the E-W direction together with a spherical expansion. On the other hand Vogel et al. (1987) and Kuan & Snyder (1994) report a southeast-northwest velocity structure in NH_3 and HNO respectively.

The presence of two hot cores with different radial velocities clarifies the inconsistencies observed in different tracers. As already discussed in Sect. 4, the final picture for the emission towards Sgr B2N as two hot cores, Sgr B2N1 and Sgr B2N2 at ~ 60 and $\sim 75\,\mathrm{kms}^{-1}$, respectively, separated by $2''$ in the north-south direction, explains the north-south velocity gradient observed in molecules like NH_3 and HNO. However the east-west velocity gradient observed in HC_3N, OCS and the H_2O masers is unclear. From the velocities and proper motions of the H_2O masers a solid rigid disk has been proposed. This is also consistent with the presence of a kinematical structure in the source as described in Sect. 7 to explain the difference in the line widths. If the HC_3N* data is to be explained by a solid rigid disk, the dynamical mass needed to bind the material in a disk which is inclined with respect to the line of sight by an angle i, and whose maximum observed velocity is v_{max} is given by:

$$M[M_\odot] = 232.49\,(v_{max}[km\,s^{-1}])^2\,r[pc]\frac{1}{\sin^2 i} \qquad (2)$$

For the inclination derived from the kinematics and proper motions of H_2O masers (Reid et al., 1988), and a maximum radial velocity of $9\,\mathrm{km\,s}^{-1}$ at a distance of $0.8''$ (0.027 pc) from the center of the source, the dynamical mass required to bind the disk is 750 $M_\odot$. This is nearly a factor 3 larger than the mass we derive in Sect. 6.3. However, the analysis of the proper motions and kinematics from the H_2O masers is based on the fact that the emission comes from one source, while the HC_3N* data clearly shows that there are two hot cores. Another possibility is that HC_3N* may come from a cluster of hot cores with typical masses of $\sim 20\,M_\odot$, similar to that in Orion A, which have been formed from molecular gas with a velocity gradient. The star formation may have been triggered by the nearby HII regions and the hot cores now reflect the kinematics of these regions. In fact, the morphology of the hot cores in Fig. 5 resemble that of the southern edge of HII region K5. Higher angular resolution observations are needed to distinguish between the two different scenarios.

9.2. Sgr B2M

As stated for Sgr B2N the trend of HC_3N* line widths in Sgr B2M would also be consistent with the kinematics of a solid rigid. The dynamical mass required to bind the material in this case would be $\sim 400\,M_\odot$, which is similar to the mass we estimated in Sect. 6.3. It may also be possible that the kinematics may be related to the velocity structure of multiple hot cores being formed in Sgr B2M. Higher angular observations are required to settle this discussion.

10. Global view of massive star formation in Sgr B2

Sgr B2 has been extensively studied in the radio continuum and in line molecular emission with very high angular resolution

and sensitivity. The number of HII regions detected in Sgr B2 is nearly 60 (Gaume et al., 1995) whereas the number of detected hot cores is only 2. This difference in the number of detections has been proposed to be due to the different lifetimes of the UC HII region phase (10^5 yr, Wood & Churchwell 1989) and the hot core phase (10^3–$6\,10^4$ yr, Kurtz et al. 2000). However the detection of typical hot cores like those in Orion either using molecular lines or dust emission requires better sensitivity than detection of UC HII regions This indicates that a complete inventory of recent massive star formation requires very sensitive observations of molecular lines or/and dust to detect all the hot cores in the region.

The results presented in this article modify the view of very recent massive star formation in the Sgr B2 cloud. It has been considered that massive stars were only forming in the main cores Sgr B2M and Sgr B2N and to a less extent in another core to the south, Sgr B2S. This view is basically based on the radiocontinuum emission and on the maser activity in the region.

We have detected four new hot cores (Sgr B2R1-B2R4) in a ridge connecting Sgr B2M and B2N and of a extended HC_3N^* emission to the west of Sgr B2M (Sgr B2W). The latter, when observed with higher angular resolution and better sensitivity, may split into even larger number of individual hot cores. This indicates that massive star formation in the Sgr B2 cloud is ongoing in the large envelope at stages previous to the HII region phase. Similar results have also been found by Martín-Pintado et al. (1999) in the southern part of the envelope of Sgr B2. The new hot cores reported in this paper, B2R1 to B2R4, and also those of Martín-Pintado (1999) are less massive than those in Sgr B2M and B2N but they are similar to those found in Orion and other regions with massive star formation.

Taking into account all data we can distinguish three star burst forming regions with massive stars at different stages of evolution, in Sgr B2M, Sgr B2N and the Sgr B2R (the ridge). The differences in evolution among these regions arise from their luminosities and the ratio between the number of HII regions and the number of hot cores.

We will refer to the Sgr B2M cluster as the region containing the F and G UC HII regions (Gaume et al., 1995). This cluster contains 23 UC HII regions, one massive hot core (~ 500 $M_\odot$) with a luminosity of $3\,10^6$ $L_\odot$ and a large H_2O maser luminosity. The abundance of HC_3N towards this core is 20 times lower than towards Sgr B2N.

The Sgr B2N cluster encompasses 7 HII regions (Gaume et al., 1995), and contains two luminous hot cores of $2\,10^7$ and $3\,10^6$ $L_\odot$ with a total mass of 800 $M_\odot$ and several H_2O masers. The Sgr B2N1 hot core shows an enhanced abundance of HC_3N. From the results of Sect. 7, the dust around the core is optically thick.

The Sgr B2 Ridge cluster is a scattered group of hot cores detected in the HC_3N^* lines, with similar luminosities to the previously-mentioned hot cores, but with a much lower masses (10-30 $M_\odot$). These hot cores are close to the HII regions X, Z, and A. Sgr B2W is also close to HII regions E, D, C, B, A and Y (Gaume et al., 1995). Only Sgr B2R2 and Sgr B2R4 seem to be associated with H_2O masers. The HC_3N abundance is similar to that found in Sgr B2N.

The fact that the Sgr B2M and Sgr B2N hot core emission is associated with two dense clusters of UC HII regions and that the H_2 column density shows its highest value in the region supports the hypothesis that these two massive hot cores may be forming a new cluster of massive stars. Arguing that a typical hot core with luminosities $L \simeq 5\,10^5$ $L_\odot$, like Orion, has a mass of $\simeq$ 10-20 $M_\odot$, the number of Orion-type hot cores in Sgr B2M and Sgr B2N (massive stars) to be found must be 20-30. This would be close to the number of HII regions already formed in the Sgr B2M cluster. The difference in the HC_3N abundance between both hot cores is probably due to the fact that the cluster of massive stars in Sgr B2N is at an earlier stage than that in Sgr B2M.

The Sgr B2R hot cores and the Sgr B2 W extended emission come from a region where HII regions are isolated or form groups of 2 or 3 individuals and the H_2 column density is 5-10 times lower than in the other two massive hot cores. These new hot cores probably represent formation of more or less isolated massive stars. However the hot cores must contain stars of similar mass and luminosity to those found in the Sgr B2M and Sgr B2N regions. The similar abundance of HC_3N in the Sgr B2 Ridge cores and Sgr B2N hot cores would suggest that they are at a similar stage of evolution.

Higher angular resolution observations with better sensitivity are necessary to reveal the number of massive stars being formed in this molecular cloud and its relation to the physical conditions of the surrounding material.

11. Conclusions

We have used the IRAM 30m telescope and the IRAM Plateu de Bure interferometer to study the hot cores at the Sgr B2 molecular cloud using several vibrationally excited HC_3N transitions. The main results derived from this work are the following:

1. A ridge of HC_3N* emission has been discovered between Sgr B2M and Sgr B2N. We distinguish four new hot core sources in the ridge labelled as Sgr B2R1, B2R2, B2R3 and B2R4. The map also shows an extended low brightness emission to the west of the ridge which we refer to as Sgr B2W.
2. The emission from the main hot cores, Sgr B2M and Sgr B2N is unresolved in our interferometric maps and we set an upper limit to the size of the cores of $3'' \times 5''$. The upper limit to the size for the ridge hot cores is $7'' \times 7''$.
3. By fitting the relative visibilities between velocity channels in our interferometric map we have obtained the relative location of the HC_3N* J=10–9,1v7,1f emission for different radial velocities towards Sgr B2N and Sgr B2M. We propose that Sgr B2N is composed of two hot cores separated $2''$ in the south-north direction, with radial velocities of 60 (Sgr B2N1) and 75 kms^{-1} (Sgr B2N2). The estimated size for both hot cores is $\sim 1.5''$.

4. The Sgr B2M hot core shows a velocity gradient. The radial velocity increases for decreasing RA. The estimated size for the hot core is $\sim 2''$.
5. The linewidths of the HC_3N* lines arising from different vibrational excited states systematically decreases for Sgr B2M and Sgr B2N1 as the energy of the vibrationally excited states increases. This kinematical effect may be due to a rotating solid rigid disk.
6. We have estimated the kinetic temperature, H_2 density, HC_3N abundance, mass and luminosity of the hot cores. Typical luminosities are 2–$3\,10^6$ $L_\odot$ for Sgr B2M and the B2R cores and $2\,10^7$ $L_\odot$ for Sgr B2N. The estimated masses for Sgr B2M and B2N are 500 and 800 $M_\odot$ respectively and $10-30$ $M_\odot$ for Sgr B2R1 to B2R4. The abundance of HC_3N towards Sgr B2M is $5\,10^{-9}$ while towards Sgr B2N1 and B2R1 to B2R4 is 1–$2\,10^{-7}$.
7. From the HC_3N* line intensities we have modeled the spatial distribution of the hot dust in the hot cores Sgr B2M and Sgr B2N. The different HC_3N abundance between Sgr B2M and Sgr B2N is probably related to the penetration of UV radiation into the hot cores and/or to time dependent chemistry. We propose that HC_3N abundance probes the evolutionary stage of the hot core.
8. We find that the excitation of the HC_3N* emission in all hot cores can be represented by a single temperature. We have developed a simple model to study the excitation of the HC_3N vibrational levels by IR radiation. We find that the single excitation temperature can be explained by high stellar luminosities ($\sim 10^7$ $L_\odot$) and small source sizes ($\sim 2-3''$).
9. The Sgr B2M and B2N hot cores are likely forming a new cluster of massive stars. If the typical mass of a hot core like Orion has 20 $M_\odot$ the number of Orion-type hot cores (massive stars) to be found in Sgr B2M and Sgr B2N must be 20, close to the number of HII regions already formed in the Sgr B2M and Sgr B2N cluster.
10. The Sgr B2R hot cores probably represent formation of isolated massive stars. However the hot cores must contain stars of similar mass and luminosity to those found in Sgr B2M and Sgr B2N.

Acknowledgements. We would like to greet the IRAM staff, and operators for their help during observations. We are also very grateful to Dr. P.F. Goldsmith, for a critical reading which substantially improved this paper. This work has been partially supported by the CYCIT and the PNIE under grants PB96-104, 1FD97-1442 and ESP99-1291-E.

References

Carlstrom, J. E. and Vogel, S. N., 1989, ApJ 337, 408
Caselli, P., Hasegawa, T. I., and Herbst, E., 1993, ApJ 408, 548
Cesaroni, R., Felli, M., Testi, L., Walmsley, C. M., and Olmi, L., 1997, A&A 325, 725
de Pree, C. G., Gaume, R. A., Goss, W. M., and Clausse n, M. J., 1995, ApJ 451, 284
de Pree, C. G., Goss, W. M., and Gaume, R. A., 1998, ApJ 500, 847
de Vicente, P., Martín-Pintado, J., and Wilson, T. L., 1997, A&A 320, 957
de Vicente P., 1994, Ph.D. thesis, Universidad Complutense de Madrid, Madrid, Spain
Gaume, R. A. and Claussen, M. J., 1990, ApJ 351, 538
Gaume, R. A., Claussen, M. J., de Pree, C. G., Goss, W. M., and Mehringer, D. M., 1995, ApJ 449, 663
Goldsmith, P. F., Krotkov, R., and Snell, R. L., 1985b, ApJ 299, 405
Goldsmith, P. F. and Langer, W. D., 1999, ApJ 517, 209
Goldsmith, P. F., Lis, D. C., Hills, R., and Lasenby, J., 1990, ApJ 350, 186
Goldsmith, P. F., Snell, R. L., Deguchi, S., Krotkov, R., and Linke, R. A., 1982, ApJ 260, 147
Goldsmith, P. F., Snell, R. L., and Lis, D. C., 1987, ApJ Lett. 313, L5
Houghton, S. and Whiteoak, J. B., 1995, MNRAS 273, 1033
Kobayashi, H., Ishiguro, M., Chikada, Y., Ukita, N., Morita, K. I., Okumura, S. K., Kasuga, T., and Kawabe, R., 1989, PASJ 41, 141
Kuan, Y. and Snyder, L. E., 1994, ApJS 94, 651
Kurtz S., Cesaroni R., C. E. H. P. W. C. M., 2000, in A. B. V. Manings and S. Russel (eds.), Protostars and Planets IV, Proc. of Protostars and Planets, University of Arizona Press
Lis, D. C. and Goldsmith, P. F., 1990, ApJ 356, 195
Lis, D. C. and Goldsmith, P. F., 1991, ApJ 369, 157
Lis, D. C., Goldsmith, P. F., Carlstrom, J. E., and Scoville, N. Z., 1993, ApJ 402, 238
Liu, S. Y. and Snyder, L. E., 1999, ApJ 523, 683
Martín-Pintado, J., De Vicente, P., Wilson, T. L., and Johnston, K. J., 1990, A&A 236, 193
Martín-Pintado, J., Gaume, R. A., Rodríguez-Fernández, N., de Vicente, P., and Wilson, T. L., 1999, ApJ 519, 667
Martín-Pintado, J., Gomez-Gonzalez, J., Delromero, A., Planesas, P., and Bujarrabal, V., 1986, in Spaceborne Submillimeter Astronomy Mission. A Cornerstone of the ESA Long Term Science Program, pp 191–194
Mehringer, D. M., Goss, W. M., and Palmer, P., 1995, ApJ 452, 304
Mehringer, D. M. and Menten, K. M., 1997, ApJ 474, 346
Miao, Y., Mehringer, D. M., Kuan, Y., and Snyder, L. E., 1995, ApJ Lett. 445, L59
Osorio, M., Lizano, S., and D'Alessio, P., 1999, ApJ 525, 808
Reid, M. J., Schneps, M. H., Moran, J. M., Gwinn, C. R., Genzel, R., Downes, D., and Roennaeng, B., 1988, ApJ 330, 809
Rodríguez-Franco, A., Martín-Pintado, J., and Fuente, A., 1998, A&A 329, 1097
Thronson, H. A., J. and Harper, D. A., 1986, ApJ 300, 396
Vogel, S. N., Genzel, R., and Palmer, P., 1987, ApJ 316, 243
Wilson, T. L. and Rood, R., 1994, ARA&A 32, 191
Wood, D. O. S. and Churchwell, E., 1989, ApJS 69, 831
Wyrowski, F., Schilke, P., and Walmsley, C. M., 1999, A&A 341, 882